Published in final edited form as:
Science. 2013 July 19; 341(6143): 1238303. doi:10.1126/science.1238303.

Tight coordination of protein translation and heat shock factor 1 activation supports the anabolic malignant state

Sandro Santagata[1,2,#], **Marc L. Mendillo**[2,3,#], **Yun-chi Tang**[3,4,†], **Aravind Subramanian**[5], **Casey C. Perley**[2,3], **Stéphane P. Roche**[6], **Bang Wong**[5], **Rajiv Narayan**[5], **Hyoungtae Kwon**[2,3], **Martina Koeva**[2,3], **Angelika Amon**[3,4], **Todd R. Golub**[5], **John A. Porco Jr.**[6], **Luke Whitesell**[2,*], and **Susan Lindquist**[2,3,*]

[1]Department of Pathology, Brigham and Women's Hospital, and Harvard Medical School, Boston, MA, USA

[2]Whitehead Institute for Biomedical Research, Cambridge, MA, USA

[3]Howard Hughes Medical Institute, Department of Biology, Massachusetts Institute of Technology, Cambridge, MA, USA

[4]David H. Koch Institute for Integrative Cancer Research and Howard Hughes Medical Institute, Massachusetts Institute of Technology, Cambridge, MA, USA

[5]Broad Institute of MIT and Harvard, Cambridge, MA, USA

[6]Department of Chemistry, Center for Chemical Methodology and Library Development (CMLD-BU), Boston University, Boston MA, USA

Abstract

A unifying characteristic of aggressive cancers is a profound anabolic shift in metabolism to enable sustained proliferation and biomass expansion. The ribosome is centrally situated to sense metabolic states but whether it impacts systems that promote cellular survival is unknown. Here, through integrated chemical-genetic analyses, we find that a dominant transcriptional effect of blocking protein translation in cancer cells is complete inactivation of heat shock factor 1 (HSF1), a multifaceted transcriptional regulator of the heat-shock response and many other cellular processes essential for tumorigenesis. Translational flux through the ribosome reshapes the transcriptional landscape and links the fundamental anabolic processes of protein production and energy metabolism with HSF1 activity. Targeting this link deprives cancer cells of their energy and chaperone armamentarium thereby rendering the malignant phenotype unsustainable.

Keywords

HSP90; aneuploidy; ribosome; mTOR; PI3Kinase; tRNA; NF1; TXNIP; translation initiation; eukaryotic initiation factors; eIF4a; rocaglates; rocaglamide A; LINCS; Large Scale Expression Analysis of Cellular States; connectivity; CMAP; proteasome

[*]Correspondence should be addressed to L.W., whitesell@wi.mit.edu or S.L., lindquist_admin@wi.mit.edu.
[†]Current address: Institute of Health Sciences, Shanghai Institutes for Biological Sciences, Chinese Academy of Sciences & Shanghai Jiao Tong University School of Medicine, Shanghai, China.
[#]Equal contributions

Introduction

High-grade malignant cells commonly increase their ribosome content to boost protein production (1–4). This amplified translational capacity allows cancer cells to satisfy the increased anabolic demands associated with malignant transformation and relentless proliferation. Many different oncogenic signaling pathways are now known to converge on the ribosome to regulate its function (5, 6). There, these inputs are integrated and the net translational activity is tuned to reflect the metabolic state of the cell. Moreover, our understanding of the ribosome as a molecular machine (7–9) and of its intricate regulation (10, 11) is greatly improved. However, it is not known whether ribosomes can transduce metabolic states – that is, convey information about total protein production (i.e. protein flux through the ribosome) – to reshape transcriptional regulatory networks. This question is critical for understanding the decision-making circuitry that empowers the intrinsically anabolic nature of cancer.

Results

Inhibiting protein flux inactivates HSF1

To investigate the transcriptional effects of reducing protein flux through the ribosome in malignant cells, we analyzed the mRNA expression profiles of breast cancer cells after treatment with various inhibitors of translation elongation (anisomycin, emetine, cephaeline and cycloheximide). Dramatic changes in the transcriptome ensued and these were highly correlated across all four inhibitors (Pearson r between 0.85 to 0.97 for all pairwise correlations). Strikingly, the most strongly enriched category consisted of genes regulated by promoters that contain DNA binding motifs for the heat-shock transcription factor known as HSF1 (p value = 9.87E-7) (Fig. 1A; table S1). Of the 13,258 genes measured, the single most down-regulated mRNA was *HSPA8*, which encodes a constitutive HSP70 chaperone that folds nascent polypeptides as they emerge from the ribosome (12) (Fig. 1B; table S2). *HSPA1A*, a cancer-induced *HSP70* gene, was also amongst the ten most down-regulated mRNAs. This transcriptional response suggested that reduced flux through the ribosome causes a profound shift in the activity of heat shock factor 1 (HSF1).

We recently reported that, in a very wide range of cancers, HSF1 regulates a transcriptional network that is distinct from the conventional network activated by thermal stress (13). This cancer network includes many classic “heat-shock” genes. But it also includes a broad cadre of other genes that play critical roles in malignancy, some of which are positively regulated by HSF1 and some negatively regulated. All four inhibitors of translation elongation profoundly affected genes in the HSF1 cancer network (Fig. 1C; p value = 0.016, fig. S1). Genes that are positively regulated by HSF1 were down regulated when translational flux through the ribosome was reduced. These genes included drivers of cell proliferation and mitogenic signaling (e.g. *CENPA*, *CKS1B*, *PRKCA*), transcription and mRNA processing (e.g. *LSM2*, *LSM4*) protein synthesis (e.g. *FXR1*, *MRPL18*), energy metabolism (e.g. *MAT2A*, *SLC5A3*, *PGK1*, *MBOAT7*, *SPR*) and invasion/metastasis (e.g. *EMP2*, *LTBP1*). In a complementary fashion, genes that were negatively regulated by HSF1 were up-regulated when translational flux through the ribosome was reduced. These included genes that promote differentiation (e.g. *NOTCH2NL*), cellular adhesion (e.g. *EFEMP1*, *LAMA5*), and apoptosis (e.g. *BCL10*, *CFLAR*, *SPTAN1*).

This powerful effect of translation inhibition on HSF1-regulated transcription led us to examine the genome-wide pattern of DNA occupancy by HSF1 in breast cancer cells. After a 6 hr. exposure to cycloheximide, we performed chromatin immunoprecipitation coupled with massively parallel DNA sequencing (ChIP-Seq) using a previously validated antibody against HSF1 (13). Importantly, despite cycloheximide treatment, HSF1 protein levels

themselves remained unchanged (Fig. 1D). In striking contrast to DNA occupancy by RNA-polymerase II (which was not globally reduced), HSF1 occupancy was nearly eliminated (compare Fig. 1E to Fig. 1F; fig. S2; table S3). This held true for genes that are either positively or negatively regulated by HSF1, as well as for genes shared with the classic heat-shock response and genes specific to the HSF1 cancer program (Fig. 1F,G; table S3). Together, these data pointed to a very strong link between the activity of the ribosome and the activity of HSF1.

The LINCS database establishes translation as a potent regulator of HSF1 in cancer cells

To further investigate the link between HSF1 activity and translation, we turned to a new and extensive expression profiling resource that has been created by the Library of Integrated Network-based Cellular Signatures (LINCS) program (Fig. 2; see Materials and Methods). The LINCS database is a massive catalog of gene-expression profiles collected from human cells treated with chemical and genetic perturbagens.

We generated a query signature for HSF1 inactivation from expression profiles of breast cancer cells that had been treated with HSF1 shRNAs (13). This signature included both genes that were up-regulated by HSF1 inactivation and down-regulated by HSF1 inactivation. We compared our HSF1 query signature to LINCS expression profiles from nine cell lines that are currently the most extensively characterized in this database (Fig. 2A). Eight of these are cancer lines of diverse histopathologic origin. These lines have been treated individually with 3,866 small-molecule compounds or 16,665 shRNAs targeting 4,219 genes. The compounds employed for these gene expression profiles encompassed FDA-approved drugs and known bioactives. The shRNAs employed were directed against the known targets of these compounds, against genes in related pathways, or against other genes that have been implicated in a variety of human diseases. In all, we compared our HSF1 signature to 161,636 LINCS signatures, each generated from at least three replicates (for a total of 614,216 profiles.)

As expected, the LINCS perturbations that negatively correlated with our HSF1 inactivation signature were enriched for known activators of HSF1. They included shRNAs that target components of the proteasome. In addition, they also included compounds that inhibit the proteasome and that inhibit Hsp90 (Fig. 2B,C; table S4).

Remarkably, the LINCS perturbations that positively correlated with our HSF1 inactivation signature were most highly enriched for translation inhibitors (cephaeline, cycloheximide, emetine) (Fig. 2B,C; table S4). These perturbations were also highly enriched for compounds that target signaling pathways that regulate protein translation – PI3Kinase/mTOR inhibitors (Fig. 2B; table S4). Of the nearly two hundred gene ontology classes analyzed, the ribosome subunit family was the single most enriched (Fig. 2B,C; table S4). In addition, eukaryotic initiation factors (eIFs) and aminoacyl tRNA synthetases were also highly enriched. This unbiased analysis using the LINCS database provides a powerful demonstration of the connection between translational flux and the function of HSF1 in cancer.

An unbiased high-throughput chemical screen for HSF1 inhibitors

To find alternate ways to inhibit HSF1, we performed a large high-throughput chemical screen. We screened 301,024 compounds through the NIH Molecular Libraries Probe Center Network (MLPCN, Pubchem AID: 2118; Fig. 3A) using an HSF1-regulated reporter driven by consensus heat-shock elements (HSEs). To accommodate constraints of the high-throughput 384 well format (see Material and Methods), we employed a reporter cell line

stably transduced with a simple luminescence-based reporter and we induced HSF1 activation with a simple proteotoxic stressor (the proteasome inhibitor MG132).

Approximately 2,500 hit compounds from the primary screen, which blocked induction of the reporter, were then counter screened with an independent dual reporter cell line (Fig. 3B) to eliminate non-selective inhibitors. This second line had been stably transduced with two constructs, one encoding a green fluorescent protein (GFP) driven by HSEs and the other encoding a red fluorescent protein (RFP) driven by a doxycycline-regulated control promoter. Compounds that selectively inhibit HSF1 activity should suppress GFP expression in this cell line but should not suppress doxycycline-mediated induction of RFP. Notably, compounds that have previously been reported to selectively inhibit HSF1, such as triptolide, quercetin, KNK423 and KNK437 (14), all suppressed both reporters (fig. S3). Thus, an unexpected finding in this screening effort was that these compounds are far less specific for HSF1 than commonly assumed.

More to the point, this very large-scale and unbiased chemical screen led us, yet again, to the link between HSF1 activation and the translation machinery. By far the most potent and selective hit to emerge from the 301,024 compounds we tested was the rocaglate known as rocaglamide A (IC50 of ~50 nM for the heat shock reporter versus IC50 >1000 nM for the control reporter; Fig. 3C). This natural product inhibits the function of the translation initiation factor eIF4A, a DEAD box RNA helicase (15, 16). Presumably, it passed counter-screening in our secondary assay with the dual reporter system because translation of the doxycycline-regulated RFP control does not require the classical cap-dependent initiation complex.

To define structure-activity relationships for inhibition of the HSE reporter by rocaglamide A, we used our dual reporter system to test thirty-eight additional rocaglates (fig. S4). These included both natural products and totally synthetic analogs prepared by photocycloaddition methods (17, 18). Five hydroxamate analogs were more potent than rocaglamide A at inhibiting the HSE reporter, while retaining similar selectivity (table S5). The most potent inhibitor had an IC50 of ~20nM (fig. S4). We named this compound Rohinitib or RHT for *Ro*caglate *H*eat Shock, *Ini*tiation of *T*ranslation *I*nhi*b*itor.

Characterizing the effects of RHT on cancer cells

To validate findings from our engineered reporter system, we measured the effects of RHT on the basal expression of several endogenous HSF1-regulated transcripts (Fig. 3D; fig. S5 and S6). RHT did not reduce the transcript levels of the control housekeeping genes *B2M* and *GAPDH.* Nor did it reduce the transcript levels of *HSF1* itself (Fig. 3D; fig. S6A). However, mRNA levels of Hsp40 (*DNAJA1)* and Hsp70 genes (*HSPA1B* and *HSPA8*) dropped significantly. The most dramatically affected was the constitutively expressed *HSPA8* gene (> 90% reduction; Fig. 3D). This was also the gene that we had found to be the most strongly repressed by translation elongation inhibitors (Fig. 1B).

The effects of RHT were not due to reductions in HSF1 protein levels, which remained constant (Fig. 3E; fig. S6B). The sharp decrease in *HSP70* mRNA levels in response to RHT held true across a histologically diverse panel of human cancer cell lines (MCF7 -breast adenocarcinoma, MO91 - myeloid leukemia, CHP100 - sarcoma, and HeLa - cervical carcinoma) as well as in artificially transformed 293T kidney cells (Fig. 3D; fig. S6A,C). RHT had a much smaller effect on *HSP70* mRNA levels in proliferating but non-tumorigenic diploid cells (WI38 and IMR90) (fig. S6C).

To obtain a more direct and global view of RHT's effects on HSF1 activity, we examined genome-wide promoter occupancy by ChIP-Seq analysis. RHT virtually abolished HSF1

binding throughout the genome (Fig. 4A,B; fig. S6D; table S3). As had occurred with cycloheximide (Fig. 1F,G), RHT affected both genes that are positively regulated by HSF1 and genes that are negatively regulated by HSF1. Furthermore, it affected both classic heat-shock genes and genes unique to the HSF1 cancer program (Fig. 4A,B; table S3). The effects on HSF1 DNA occupancy occurred at concentrations of cycloheximide and RHT that inhibit the ribosome activity to a similar extent (Fig. 4C).

Rocaglates modulate tumor energy metabolism

While characterizing the effects of RHT on the transcriptome, we noted a striking inability of treated cells to acidify the culture medium (detected incidentally by the color of the pH indicator phenol red included in standard media). This suggested a reversal of the "Warburg effect", a metabolic shift responsible for increased lactic acid production by many cancers. Genetic compromise of HSF1 drives a shift in metabolism in both cell culture and animal models (19, 20). Hence this effect of RHT is consistent with inactivation of HSF1.

Strikingly, our mRNA expression profiling of rocaglate-treated breast cancer cells also revealed that mRNA levels for thioredoxin interacting protein (TXNIP) were markedly up-regulated. TXNIP is a powerful negative regulator of glucose uptake and is a well-established regulator of cellular energy status (21, 22). Its expression is dramatically reduced in malignant cells, leading to increased glucose uptake (23). Conversely, increasing TXNIP levels leads to reduced glucose uptake (21). The induction of TXNIP mRNA by RHT was observed across a diverse panel of tumor cell lines (Fig. 5A). TXNIP protein levels also increased sharply despite a marked reduction in the levels of other short-lived proteins such as p53 (Fig. 5B). While we did not detect HSF1 bound to the TXNIP locus, HSF1 did directly regulate a group of other genes involved in energy metabolism (including *MAT2A*, *SLC5A3*, and *PGK1*). At a functional level, the effects of RHT were associated with concentration-dependent reductions in both glucose uptake and lactate production (Fig. 5C). Thus, the effects of RHT on protein translation, HSF1 activation, and energy metabolism – processes lying at the core of the anabolic state of cancer – are very tightly coordinated.

Rocaglates selectively target aneuploid cancer cells and non-transformed cells with cancer-associated genetic aberrations

Does this tight coordination create vulnerabilities for the malignant phenotype that could be exploited as a therapeutic strategy? We looked at a range of cell-based cancer models unified by their increased dependence on HSF1 activation for growth and survival. Although it occurs very early during oncogenesis, simple loss of the tumor suppressor *Nf1* leads to an increase in HSF1 protein levels, nuclear localization and transcriptional activation (24). We treated mouse embryonic fibroblasts (MEFs) in which *Nf1* is knocked out and wild-type littermate control MEFs in which HSF1 is not activated, with either RHT or with cycloheximide. The two cell types were similarly sensitive to cycloheximide. However, *Nf1*-null MEFs were more sensitive than wild-type MEFs to RHT (Fig. 6A). In this model for an early event in tumorigenesis, targeting translation initiation rather than translation elongation seems to provide a more selective, better tolerated approach for disrupting the link between translation and HSF1 activation.

A second engineered system allowed us to ask if rocaglates would selectively inhibit the growth of cells carrying a simple chromosomal aberration that models another common early event in the development of cancer – aneuploidy. Chromosomal imbalances lead to both increased energy and proteotoxic stress. This is reflected by the elevation of the HSF1-regulated chaperone protein HSP72, encoded by *HSPA1A* (25). We isolated MEFs from mice carrying Robertsonian fusions for chromosome 13 (26). These MEFs (TS-13-1 and

TS-13-2) carry a single extra copy of 120Mbp of chromosome 13, thereby introducing an additional copy of 843 genes.

Cycloheximide, as well as conventional cytotoxic chemotherapeutics (i.e. taxol and hydroxyurea), inhibited the growth of both trisomic and littermate control MEFs to an equal extent (Fig. 6B, fig. S7). But, trisomic MEFs (p value <0.0001) were more sensitive than wild-type MEFs to RHT (Fig. 6B). Thus, again in this model for an early neoplastic change that activates HSF1, targeting translation initiation seems to provide a better tolerated, more selective approach for targeting the malignant state.

HSF1 activation is even more prominent in advanced malignancies (13, 27, 28). For example, colon cancers frequently show immunohistochemical evidence of strong HSF1 activation (Fig. 6C) and this correlates with poor clinical outcome (13). We mined publicly available expression profiling from colon cancer lines with highly aneuploid karyotypes (Chromosomal instability, CIN) and from colon cancer lines with near-euploid karyotypes, but microsatellite instability (MIN). The CIN lines expressed markedly higher levels of *HSPA1A,* consistent with greater levels of proteotoxic stress and greater activation of the HSF1-regulated cancer program (Fig. 6D,E). Next we tested several patient-derived colon cancer lines with CIN and several patient-derived colon cancer lines with MIN for sensitivity to inhibition by RHT. The CIN lines were much more sensitive than the MIN lines. Non-transformed colon epithelial cell lines with euploid chromosome content were the least sensitive of all the lines we tested (Fig. 6F).

Rocaglates suppress the growth of cancer cells in vitro and of tumors *in vivo*

Some rocaglates have previously been shown to exert profound anti-cancer activity (15, 29–31). We tested RHT against a collection of cell lines including non-transformed diploid lines and cancer cell lines with diverse histopathological origins and oncogenic lesions (Fig. 7A). The non-transformed cell lines were relatively resistant to RHT (IC50 from 100–300 nM). All cancer cell lines were sensitive to RHT (IC50 <30 nM) – the hematopoietic tumor cell lines were especially sensitive (IC50 ≤5 nM). We used one of these hematopoietic tumor lines, the M0-91 cell line originally derived from a patient with acute myeloid leukemia (32), to further characterize the effects of RHT. RHT strongly suppressed *HSPA8* mRNA levels in M0-91 cells and induced *TXNIP* mRNA (Fig. 7B). In addition, RHT sharply decreased glucose uptake by these cells (Fig. 7C).

Are the dramatic effects of RHT in cell culture achievable at drug exposures that are systemically tolerable in animals? To directly address this critical issue of therapeutic index, we first used standard *in vitro* assays to test whether RHT had sufficiently drug-like properties to justify testing in mice (fig. S8). We assessed aqueous solubility, plasma stability, plasma protein binding, hepatic microsome stability and cellular permeability (fig. S8A). No severe liabilities were found. We next established minimally toxic parameters for dosing mice with RHT and performed a plasma pharmacokinetic study following administration of 1 mg/kg subcutaneously (fig. S8 B,C). Peak plasma levels were far in excess of those required for the key biological activities we had demonstrated in cell culture. Moreover, levels required for anti-cancer activity *in vitro* were maintained in excess of 2 hours *in vivo*.

We next established subcutaneous tumor xenografts of the human myeloid leukemia cell line M091 in NOD-SCID immunocompromised mice. When the mean tumor volume reached 100 mm^3, we administered RHT at 1mg/kg for four consecutive days each week for three weeks (the schedule is indicated in Fig. 7D). Over the treatment period there was no evidence of gross systemic toxicity. Strikingly, RHT mediated marked, sustained inhibition of the growth of this very aggressive myeloid malignancy (Fig. 7D).

We then pursued pharmacodynamics studies. Mice bearing xenografts were given a single dose of RHT. Tumors were explanted four hours later and *HSPA8* and *TXNIP* mRNA levels were determined by RT-PCR (Fig. 7E). Similar to the effects we observed in cell culture, RHT caused a strong decrease in *HSPA8* transcript levels and a strong increase in *TXNIP* transcript levels. In a separate experiment, we monitored the uptake of fluorescently-labeled 2-deoxyglucose 48 hours post RHT dosing. RHT strongly suppressed uptake of this glucose analog by these tumors (Fig. 7F). Clearly, the dramatic effects of RHT that we had demonstrated on the anabolic state of tumor cells in cell culture can also be achieved in whole animals, thereby validating the importance of the link between translation, HSF1 activity and anabolic cancer phenotypes *in vivo*.

Discussion

We and others have previously shown that HSF1 provides essential support for the malignant state by blocking apoptotic responses and promoting protein synthesis, anabolic energy metabolism, mitogenic signaling pathways, and pathways that facilitate invasion and metastasis (13, 19, 20, 24, 28, 33–35). Here, we find that the ability of HSF1 to maintain this cancer program is exquisitely sensitive to the activity of the ribosome.

Our work establishes that the ribosome functions as a central information hub: translational flux conveys information about the cell's metabolic status to regulate the transcriptional programs that support it. The specific molecular mechanisms by which these effects are achieved are sure to be multifaceted, but HSF1 is clearly a linchpin in this information circuit. It is centrally poised to support protein folding and biomass expansion as well as many other functions to which malignant cells are addicted (13, 19, 20, 36). We postulate that the ribosome/HSF1 link we have uncovered in cancer may derive from ancient systems geared to align and synchronize essential cellular functions for growth and survival. In this respect it is notable that in the nematode, HSF1 is a longevity factor and in yeast, is an essential gene that participates in co-translational quality control (37–39).

In man, the ribosome/HSF1 circuit is particularly important in supporting the malignant phenotype as it can respond to varied metabolic inputs that are commonly dysregulated in cancer (5, 6, 40–42). This ribosome/HSF1 link allows these metabolic inputs to bolster the cytoprotective milieu, thereby helping tumor cells to accommodate the drastic internal imbalances arising during oncogenesis as well as the severe external stresses arising from therapeutic interventions (43). The tight coordination of protein translation and HSF1 activation, together with the many ways that cells integrate the derangements of malignancy with ribosome activity, suggests that unifying principles drive HSF1 activation across the extraordinarily wide range of human cancers in which that activation occurs (13, 27).

While cancer cells often co-opt powerful, adaptive non-oncogene systems for their benefit (44), it now appears that by co-opting the ribosome/HSF1 circuit, cancers become especially vulnerable to agents that target translation and its upstream regulatory pathways. In this regard, our animal experiments suggest that targeting translation initiation may offer a selective strategy for reversing HSF1 activation and for thereby disabling the metabolic and cytoprotective addictions of malignant cells.

Materials and Methods

Cell lines

WI38, CHP100, HeLa, 293T, PC3, MCF7, and NIH3T3 cells were purchased from American Type Culture Collection (ATCC). Immortalized *Nf1* knockout mouse embryonic fibroblasts (MEF) and littermate wild-type control MEF were kind gifts from Karen

Cichowski. Littermate-derived euploid and trisomic primary mouse embryonic fibroblasts (MEFs) were described previously (25). RHT treatments experiments were performed using chromosome 13 trisomic cell lines and using littermate control euploid cell lines that carried a single Robertsonian translocation. Early passage MEFs were used to ensure that additional karyotypic changes had not yet occurred. Two primary human cell lines (CCD112 CoN, CCD841 CoN), five MIN lines (HCT-116, HCT-15, DLD-1, SW48 and LoVo), and five CIN lines (Caco2, HT-29, SW403, SW480 and SW620) were obtained from ATCC. Chromosome number and karyotype information was obtained from the NCI database and the COSMIC Dataset at the Sanger Institute. M0-91 cells were previously described (32). The M0-91 cell line used in this study were established from explanted M0-91 tumors that had been xenografted once in mice. All cell cultures were maintained under 5% CO2 in media according to their specifications.

mRNA expression profiling and analysis

Expression profiles for MCF7 cells treated for 6 hrs. with anisomycin (15 μM), emetine (7 μM), cephaeline (6 μM) and cycloheximide (14 μM) were previously deposited in the Connectivity Map (46). MCF7 cells were treated with 200 nM rocaglamide A or 50 nM RHT for 6 hrs. and RNA was then purified following extraction with TRIzol reagent (Invitrogen, cat. #15596-026). Gene expression analysis was performed using Affymetrix GeneChip HT Human Genome U133A 96-Array Plates and data was analyzed as previously described (13). All microarray raw data were deposited in a public database (NCBI Gene Expression Omnibus pending). Gene set enrichment analysis of the differentially expressed genes following treatment of MCF7 cells with translation elongation inhibitors was performed using the Molecular Signatures Database (MSigDB) (45). Enrichment for HSF1-bound genes among the genes differentially expressed after treatment of MCF7 cells with translation elongation inhibitors was conducted using GSEA v2.08 software (45). HSF1 bound genes in MCF7 cells were defined as those genes bound in at least two of the four datasets (two datasets from this study and two from (13)).

Evaluation of *HSPA1A* mRNA levels was performed using data from the GSK Cancer Cell Line Genomic Profiling Data https://cabig.nci.nih.gov/community/tools/caArray. MIN lines used were HCT15, LS174T, SW48. CIN lines used were NCIH508, NCIH747, SW1116, SW1417, SW403, SW480, SW620, T84, SW948.

ChiP-Seq and ChIP-PCR

Described in Supplemental Materials and Methods.

Immunoblot

Described in Supplemental Materials and Methods.

LINCS analysis

To identify chemical and genetic modulators that are correlated with HSF1 inactivation we queried the Library of Integrated Cellular Signatures (LINCS) supported by the NIH Common Fund. This resource at the Broad Institute is a massive expression profiling initiative to catalog the cellular consequences of both small molecule and genetic perturbations. The expression data was generated using a high-throughput luminex bead based platform as described previously (47).

For the analysis we generated an HSF1 inactivation signature (table S4) of the 50 genes most positively regulated (reduced expression upon HSF1 depletion with shRNA) and 10 genes most negatively regulated (increased expression upon HSF1 depletion with shRNA) in

the breast cancer cell lines, MCF7 and BPLER (48) (average of the difference between the ha6 shRNA and scrambled shRNA control values between the two cell lines; (13)), that were also bound by HSF1 in our ChIP-seq experiments. This signature was used to query all 161,636 shRNA and compound signatures (collapsed from a total of 614,216 individual profiles from at least 3 biological replicates) in the LINCS dataset produced in nine cell lines (MCF7 – breast cancer, HT29 - colon cancer, HEPG2 -hepatoblastoma, A549 - lung cancer, HCC515 - lung cancer, A375 - melanoma, PC3- prostate cancer, VCAP - prostate cancer, HA1E - immortalized but non-transformed kidney epithelium). A connectivity score was assigned to each of the expression profiles from the 161,636 perturbations based on a weighted kolmogorov-smirnov statistic as previously described (45, 47). Gene set enrichment analysis (GSEA) (45) was performed on this rank-ordered list to determine gene or chemical classes that were most enriched among the positively and negatively connected signatures. The sets analyzed by GSEA encompassed the shRNAs corresponding to the genes comprising all 186 KEGG pathway gene sets. The sets also included 110 chemical classes grouped according to the Anatomical Therapeutic Chemical (ATC) Classification System. In addition, we added a set composed of elongation initiation factors. Statistical significance was tested by using 100 random sets size matched to the set being tested.

Reporter cell lines

Y9 reporter NIH3T3 cells (49) were infected with lentivirus for the doxycycline regulatable pTRIPZ-nonsilencing construct (RHS4743). These cells were heat shocked and incubated with doxycycline and then sorted by flow cytometry to isolate strong eGFP and tRFP expressors. Sorting was repeated twice for enrichment. Non-induced cells were sorted to remove cells expressing eGFP and tRFP at baseline to make R4.1.B4 cells. To make the high-throughput screening cell line NIH3T3HGL, the parent vector LV-eGFPfLUC was modified by removing the CMV promoter and introducing a 470bp fragment of the human HSP70B' construct upstream of the eGFP promoter. NIH3T3 cells were infected with lentivirus generated from this construct and the high eGFP expressors were isolated by flow cytometry following heat shock.

High-throughput small molecule screen

Described in Supplemental Materials and Methods.

Dual reporter cell assay

Described in Supplemental Materials and Methods.

Rocaglamide/rocaglate derivatives

Rocaglamide/rocaglate derivatives were prepared by total synthesis methods as previously described (17, 18).

Nanostring/nCounter analysis

The cells were lysed at concentration of 10,000 cells/μL with RTL buffer (Qiagen cat. #79216) and dissociated using a cell shredder (Qiagen cat. #79656). The total RNA in 5 μl of lysate was hybridized with the capture and reporter probes overnight at 65°C and processed according to the nCounter recommended protocol. Target/probe complexes were immobilized in nCounter Cartridges for data collection using an nCounter Digital. The data was analyzed according to the manufacture's guidelines.

S35 labeling

MCF7 cells were grown to confluence in 6 well dishes in standard DMEM (+10% FBS). The cells were rinsed twice in 1X PBS and then placed in DMEM without methionine or

cysteine (Life Technologies # 21013024) for 30 mins. EASYTAG(TM) S35 protein labeling mix (NEG772002MC) was added for 15 mins. The cells were rinsed twice in 1X PBS and then lysed in TNEK buffer. Cell lysates were prepared in TNEK buffer (50 mM Tris, pH 7.4; NP-40 1%; EDTA 2 mM; KCl 200 mM and protease inhibitor cocktail (Roche Diagnostics, cat. #11836153001). Samples (15 μg total protein/lane) were analyzed by SDS-PAGE. The gel was incubated for 10 mins in 0.7M Sodium Salicylate and 10% glycerol. The dried gel was used to expose film. Counts per minute were assessed using a scintillation counter.

Glucose uptake

500,000 cells plated in 24 well tissue culture plates were treated for 8 hrs. with RHT. The cells were then washed in 1xPBS (x2) and placed in glucose-free and serum-free DMEM for 20 min. Glucose uptake was measured using ^{3}H-2-Deoxyglucose (^{3}H-2DG), incubation for 15 minutes (final 1 μCi/ml, 50 μM 2DG). The cells were washed with 1 ml of cold 1xPBS (x2), lysed with 0.2 M sodium hydroxide and then counted by scintillation. Experiments were performed in triplicate. Parallel treated cultures cells were stained with Sytox-green (Invitrogen, cat. # S7020) for normalization. Each analysis was performed three times. The standard error of the mean is displayed.

Glucose uptake was also measured using IRD800 2-Deoxyglucose (in Fig. 7C). M0-91 cells were washed and resuspended in glucose-free medium (10e6 cells/ml). Cells were dispensed (100 μL/well) in triplicate wells and incubated for 20 mins with 5 μM of the IRDye 800CW 2-DG Optical Probe LI-COR Biosciences cat. #926-08946). The cells were then washed X4 with cold PBS and the signal was acquired using an infrared Odyssey imaging system (LI-COR Biosciences).

Lactate production

500,000 cells were plated in 24 well tissue culture plates and were treated for 8 hrs. with RHT. Following two washes with 1x PBS, the cells were incubated for 30 mins at 37°C in 500 μl of filter sterilized 1x Krebs buffer (126 mM NaCl, 2.5 mM KCl, 1.2 mM NaH2PO4, 1.2 mM MgCl2, 2.5 mM CaCl2, 10 mM Glucose, 25 mM NaHCO3, 10 mM HEPES-KOH pH 7.4). The supernatant was collected and the lactate was measured with a Lactate Assay Kit (BioVision, cat. # K-607) according to the manufacturer's guidelines. Parallel treated cultures cells were stained with Sytox Green (Invitrogen, cat. # S7020) for normalization. Each analysis was performed three times. The standard error of the mean is displayed.

Cell viability assay

Relative cell growth and survival was measured in 96-well microplate format using the fluorescent detection of resazurin dye reduction as an endpoint (544 nm excitation and 590 nm emission). 2,000 adherent cells and 10,000 suspension cells were plated 24 hrs. prior to compound exposure (for 72 hrs.). Each analysis was performed three times. For all bar graphs, the standard error of the mean is displayed, unless indicated otherwise.

Immunohistochemistry

Paraffin blocks of human colon adenocarcinoma tissue were obtained from the archives of BWH in accordance with the regulations for excess tissue use stipulated by the BWH institutional review board. Immunohistochemistry for HSF1 was performed as previously described (13).

Drug metabolism and pharmacokinetic studies

Described in Supplemental Materials and Methods.

Xenograft experiment

5e7 M0-91 cells were implanted with Matrigel (BD Biosciences) subcutaneously in the right inguinal region of NOD-SCID mice. When the mean tumor volume reached 100 mm^3, RHT formulated in hydroxypropyl beta-cyclodextrin was administered by subcutaneous parenteral administration (1 mg/kg) according to the treatment schedule shown in Fig. 7D. Tumor size was measured twice each week by a lab member (M.D.) who was blinded to the treatment groups. There were 8 mice in each treatment group (RHT treated or vehicle treated).

In vivo glucose uptake experiment

M0-91 cells were inoculated into the inguinal region of NOD-SCID mice. 17 days later, the mice were treated with a dose of RHT (1 mg/kg; 4 mice) or vehicle control (4 mice). Four hours later the mice were given retro-orbital injections of 100 μl IRDye 800CW 2-DG Optical Probe (10nmol; #926-08946 LI-COR Biosciences) and then an additional 4 hours later these mice were again treated with RHT (1mg/kg) or vehicle control. 36 hours after the last RHT dose, mice were imaged (IVIS; excitation 745 nm, emission 800 nm). Data was analyzed using Living Image software.

Real time PCR

RNA was purified with RNEasy columns (Qiagen, cat. 74104). Quantitative PCR to evaluate mRNA levels was performed using RT2 SYBR Green qPCR Mastermix (SABiosciences) and primer assay pairs (SABiosciences; Valencia, CA) on a 7900HT ABI Detection System.

Supplementary Material

Refer to Web version on PubMed Central for supplementary material.

Acknowledgments

We thank T. Volkert, J. Love, S. Gupta, and the WIBR-GTC for sequencing support, S. Malstrom (Koch Institute for Integrative Cancer Research) for assistance with *in vivo* imaging, G. Bell, P. Thiru and A. Lancaster for assistance with informatics analysis, the Connectivity Map team at the Broad Institute for generation of the LINCS dataset and query tools, Joe Negri and the MLPCN team at the Broad Institute for chemical screening and M. Duquette for assistance with animal experiments. We also thank C. Rodrigo (Boston University) for compound synthesis. We thank the Lindquist lab for helpful discussions and suggestions. The work was supported by the J&J COSAT focused funding program (L.W.) and the Marble Fund (S.L.). The MLPCN screen was supported by R03 MH086465-01 and R03 DA027713-01 to L.W.. This work was supported by the NIH Common Fund's Library of Integrated Network-based Cellular Signatures (LINCS) program (5U54HG006093, "Large scale gene expression analysis of cellular states") to T.R.G.. J.A.P. Jr. is supported by R01 GM073855. S.L. is an Investigator of the Howard Hughes Medical Institute. M.L.M. was supported by American Cancer Society New England Division-SpinOdyssey (PF-09-253-01-DMC). S.S. is supported by NIH (K08NS064168), the Brain Science Foundation, the American Brain Tumor Association, the Beez Foundation, the V Foundation and the Jared Branfman Sunflowers for Life Fund.

References

1. Ruggero D, Pandolfi PP. Nat Rev Cancer. Mar.2003 3:179. [PubMed: 12612653]
2. Chan JC, et al. Sci Signal. Aug 30.2011 4:ra56. [PubMed: 21878679]
3. White RJ. Nat Rev Mol Cell Biol. Jan.2005 6:69. [PubMed: 15688068]
4. Hannan KM, et al. Mol Cell Biol. Dec.2003 23:8862. [PubMed: 14612424]
5. Silvera D, Formenti SC, Schneider RJ. Nat Rev Cancer. Apr.2010 10:254. [PubMed: 20332778]
6. Roux PP, Topisirovic I. Cold Spring Harb Perspect Biol. 2012; 4
7. Steitz TA. Nat Rev Mol Cell Biol. Mar.2008 9:242. [PubMed: 18292779]

8. Klinge S, Voigts-Hoffmann F, Leibundgut M, Arpagaus S, Ban N. Science. Nov 18.2011 334:941. [PubMed: 22052974]
9. Ben-Shem A, et al. Science. Dec 16.2011 334:1524. [PubMed: 22096102]
10. Sonenberg N, Hinnebusch AG. Cell. Feb 20.2009 136:731. [PubMed: 19239892]
11. Hsieh AC, et al. Nature. May 3.2012 485:55. [PubMed: 22367541]
12. Hartl FU, Hayer-Hartl M. Science. Mar 8.2002 295:1852. [PubMed: 11884745]
13. Mendillo ML, et al. Cell. Aug 3.2012 150:549. [PubMed: 22863008]
14. Whitesell L, Lindquist S. Expert Opin Ther Targets. Apr.2009 13:469. [PubMed: 19335068]
15. Bordeleau ME, et al. J Clin Invest. Jul.2008 118:2651. [PubMed: 18551192]
16. Chambers JM, et al. Org Lett. Mar 15.2013 15:1406. [PubMed: 23461621]
17. Rodrigo CM, Cencic R, Roche SP, Pelletier J, Porco JA. J Med Chem. Jan 12.2012 55:558. [PubMed: 22128783]
18. Roche SP, Cencic R, Pelletier J, Porco JA Jr. Angew Chem Int Ed Engl. Sep 3.2010 49:6533. [PubMed: 20687060]
19. Jin X, Moskophidis D, Mivechi NF. Cell Metab. Jul 6.2011 14:91. [PubMed: 21723507]
20. Dai C, Whitesell L, Rogers AB, Lindquist S. Cell. Sep 21.2007 130:1005. [PubMed: 17889646]
21. Parikh H, et al. PLoS Med. May.2007 4:e158. [PubMed: 17472435]
22. Stoltzman CA, et al. Proc Natl Acad Sci U S A. May 13.2008 105:6912. [PubMed: 18458340]
23. Kim SY, Suh HW, Chung JW, Yoon SR, Choi I. Cell Mol Immunol. Oct.2007 4:345. [PubMed: 17976314]
24. Dai C, et al. J Clin Invest. Oct 1.2012 122:3742. [PubMed: 22945628]
25. Tang YC, Williams BR, Siegel JJ, Amon A. Cell. Feb 18.2011 144:499. [PubMed: 21315436]
26. Williams BR, et al. Science. Oct 31.2008 322:703. [PubMed: 18974345]
27. Santagata S, et al. Proc Natl Acad Sci U S A. Nov 8.2011 108:18378. [PubMed: 22042860]
28. Fang F, Chang R, Yang L. Cancer. Apr 1.2012 118:1782. [PubMed: 22009757]
29. Alinari L, et al. Clin Cancer Res. Sep 1.2012 18:4600. [PubMed: 22791882]
30. Cencic R, et al. PLoS One. 2009; 4:e5223. [PubMed: 19401772]
31. Lucas DM, et al. Blood. May 7.2009 113:4656. [PubMed: 19190247]
32. Okabe M, et al. Leuk Res. Dec.1995 19:933. [PubMed: 8632663]
33. Meng L, Gabai VL, Sherman MY. Oncogene. Sep 16.2010 29:5204. [PubMed: 20622894]
34. Santagata S, et al. ACS Chem Biol. Feb 17.2012 7:340. [PubMed: 22050377]
35. Scott KL, et al. Cancer Cell. Jul 12.2012 20:92. [PubMed: 21741599]
36. Westerheide SD, Anckar J, Stevens SM Jr, Sistonen L, Morimoto RI. Science. Feb 20.2009 323:1063. [PubMed: 19229036]
37. Brandman O, et al. Cell. Nov 21.2012 151:1042. [PubMed: 23178123]
38. Hahn JS, Hu Z, Thiele DJ, Iyer VR. Mol Cell Biol. Jun.2004 24:5249. [PubMed: 15169889]
39. Hsu AL, Murphy CT, Kenyon C. Science. May 16.2003 300:1142. [PubMed: 12750521]
40. Chou SD, Prince T, Gong J, Calderwood SK. PLoS One. 2012; 7:e39679. [PubMed: 22768106]
41. Hensen SM, et al. Cell Stress Chaperones. Nov.2012 17:743. [PubMed: 22797943]
42. Peng T, Golub TR, Sabatini DM. Mol Cell Biol. Aug.2002 22:5575. [PubMed: 12101249]
43. Whitesell L, Santagata S, Lin NU. Curr Mol Med. Jul 17.2012
44. Solimini NL, Luo J, Elledge SJ. Cell. Sep 21.2007 130:986. [PubMed: 17889643]
45. Subramanian A, et al. Proc Natl Acad Sci U S A. Oct 25.2005 102:15545. [PubMed: 16199517]
46. Lamb J, et al. Science. Sep 29.2006 313:1929. [PubMed: 17008526]
47. Peck D, et al. Genome Biol. 2006; 7:R61. [PubMed: 16859521]
48. Ince TA, et al. Cancer Cell. Aug.2007 12:160. [PubMed: 17692807]
49. Turbyville TJ, et al. J Nat Prod. Feb.2006 69:178. [PubMed: 16499313]

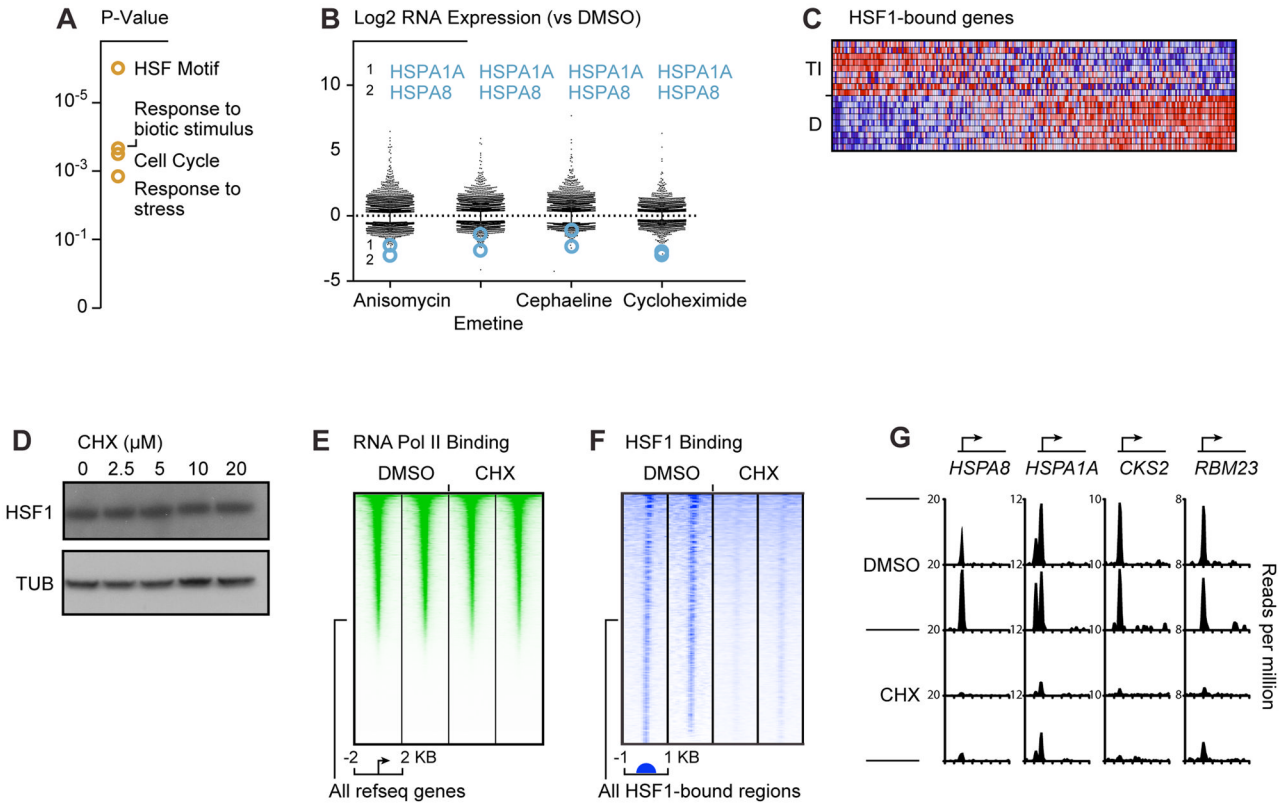

Fig. 1. Inhibiting protein flux inactivates HSF1

(**A**) Gene set enrichment analysis was performed by using the MSigDB web service (http://www.broadinstitute.org/gsea/index.jsp) on genes negatively regulated in breast cancer cells following a 6 hr. incubation with inhibitors of protein translation elongation. Complete GSEA results are provided in table S1. (**B**) Scatter plot of levels of mRNA transcripts (log2) following a 6 hr. incubation with the indicated inhibitors of protein translation elongation. The levels of HSPA1A and HSPA8 levels are indicated for each elongation inhibitor. (**C**) Translation elongation inhibitors alter the basal transcriptional program in breast cancer cells. Genes bound by HSF1 in MCF7 were ranked by their differential expression between cells treated with translation elongation inhibitors (TI) and control DMSO. Each column represents a gene and is normalized across the column, with high expression in red and low expression in blue. (**D**). An immunoblot shows the levels of HSF1 protein and the loading control tubulin after a 6 hr. exposure to the indicated concentrations of cycloheximide (CHX). (**E**) Heat map of RNA polymerase II ChIP-Seq read density in MCF7 cells that were treated with DMSO or 10 μM CHX for 6 hrs. Genomic regions from −2kb to +2kb relative to the transcription start site for all RefSeq genes are shown. (**F**) Heat map of HSF1 ChIP-Seq read density in MCF7 cells that were treated with DMSO or 10 μM CHX for 6 hrs. Genomic regions from −1kb to +1kb relative to the peak of HSF1 binding for all HSF1 enriched regions (union of all HSF1 enriched regions in the four data sets depicted here) are shown. (**G**) Representative genes bound by HSF1 in MCF7 cells (*HSPA8*, *HSPA1A*, *CKS2*, and *RBM23*). x-axis: from 2kb from the transcription start site (TSS) to 5 kb from the TSS for each gene.

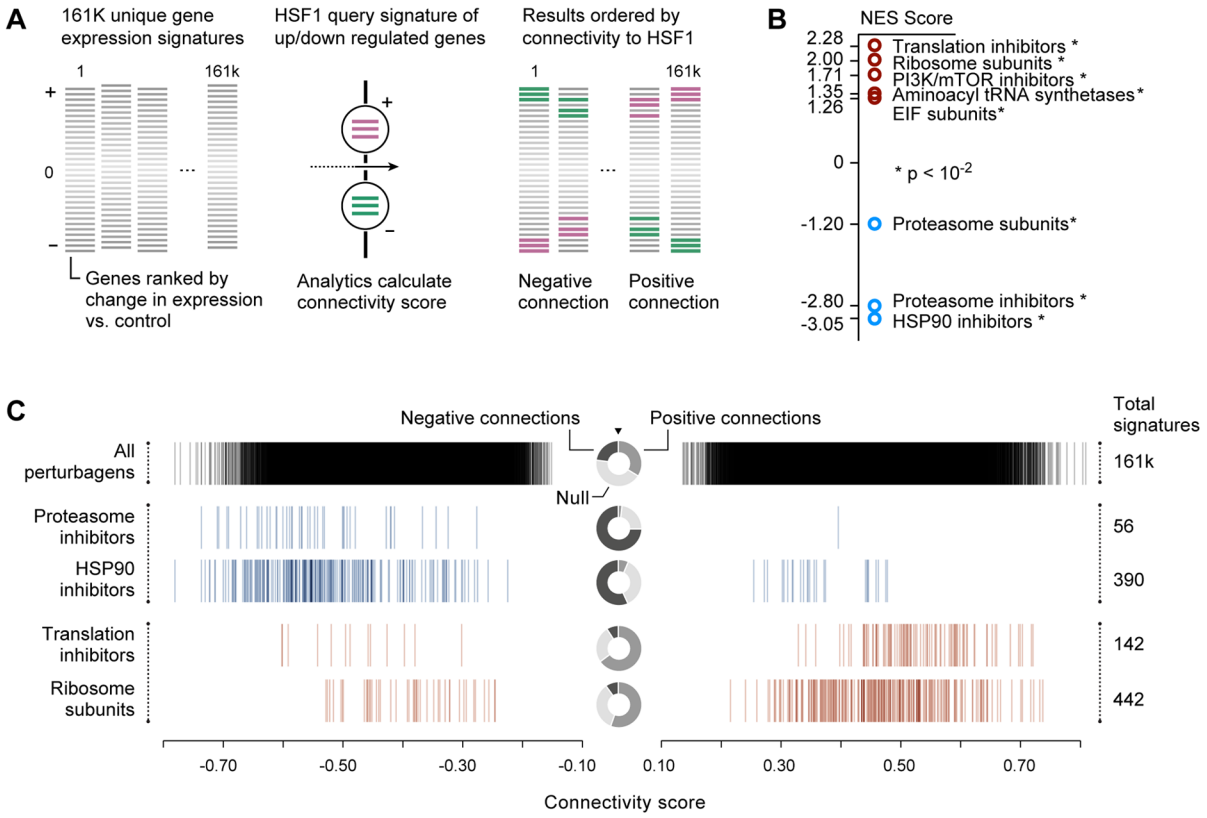

Fig. 2. LINCS analysis reveals that targeting protein translation inactivates HSF1

A. Schematic representation of the LINCS analysis used to identify chemical and genetic modulators that are correlated with HSF1 inactivation. Pink represents genes whose levels increase and green represents genes whose levels decrease following shRNA mediated knockdown of HSF1. B. GSEA results of our HSF1 inactivation signature LINCS analysis. Perturbation signatures were rank-ordered by connectivity with the HSF1 inactivation signature and enrichment was determined for KEGG pathway gene sets and ATC chemical classes (see Materials and Methods for details). Normalized enrichment score (NES) of selected results are plotted (complete GSEA results are provided in table S4). C. Barcode plot of the connectivity score of all of the individual perturbations comprising the indicated enriched chemical or gene sets. The bagel plot in the center of the barcode plot summarizes the positive, negative and null (not connected) fractions for the indicated enriched class. All perturbations that are positively or negatively connected for the indicated enriched classes are shown. Total perturbations in each class are indicated on the right of the plot. Blue represents negatively connected and red represents positively connected classes of enriched perturbations.

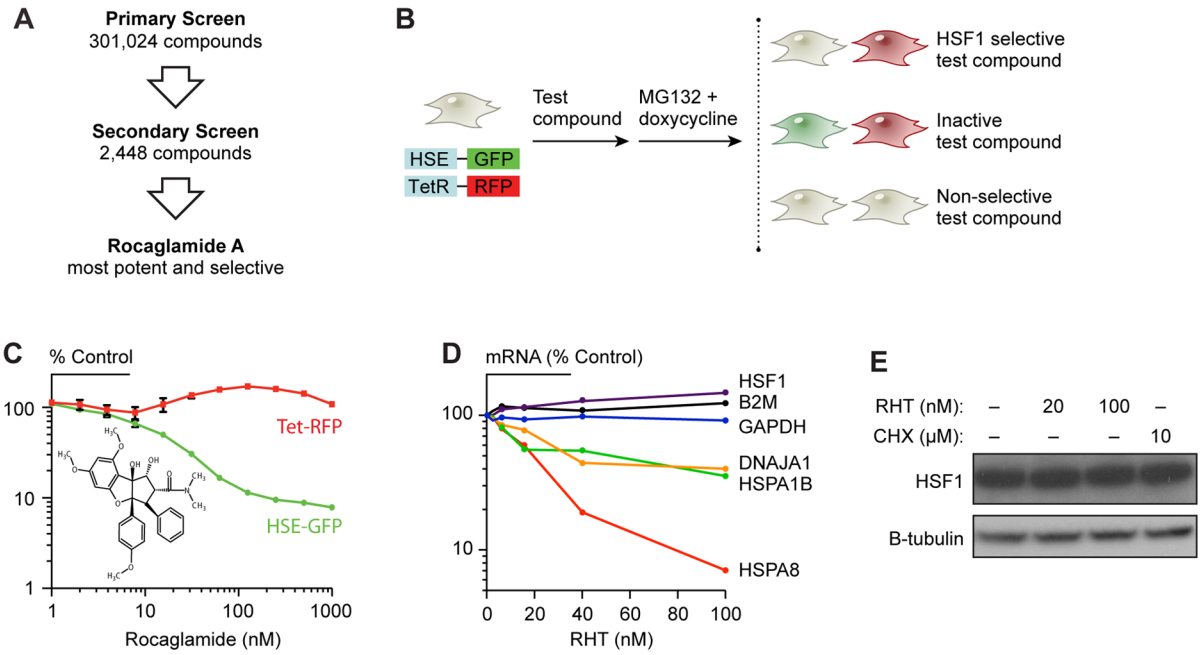

Fig. 3. Chemical screens reveal that targeting translation control inactivates HSF1

(**A**) Flowchart outlining the steps in the high-throughput MLPCN screen for inhibitors of HSF1 activation. (**B**) Schematic of dual reporter cell line used to counter-screen primary screen hits. GFP expression is regulated by a heat shock inducible promoter. RFP expression is regulated by a doxycycline response element (TetR). (**C**) Effect of rocaglamide A on the HSE-driven GFP and doxycycline-driven RFP signals following incubation with 2.5 mM MG132 and 2 μg/ml doxycycline. Chemical structure of rocaglamide A is displayed in the inset. (**D**) Effect of RHT on HSF1-regulated and control endogenous mRNA transcript levels in M0-91 leukemia cells measured by nanostring nCounter following 6 hr. incubation with indicated concentrations of RHT. Levels of endogenous transcript are shown as percent of DMSO treated control. (**E**) HSF1 protein levels are not affected in M0-91 leukemia cells treated with RHT. Immunoblot shows the levels of HSF1 protein and the loading control (Tubulin) after a 6 hr. exposure to the indicated concentrations of RHT.

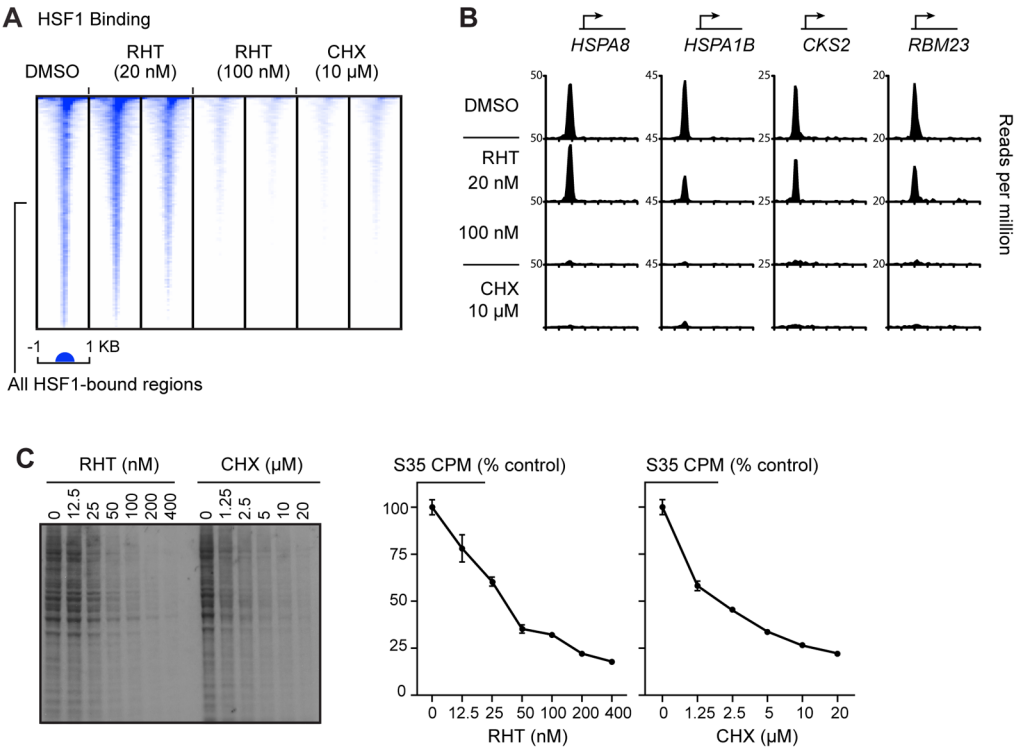

Fig. 4.

(**A**) Heat map of HSF1 ChIP-Seq read density in M0-91 cells that were treated with DMSO, 20 nM RHT, 100 nM RHT or 10 μM CHX for 6 hrs. Genomic regions from −1kb to +1kb relative to the peak of HSF1 binding for all HSF1 enriched regions (union of all HSF1 enriched regions in the seven data sets depicted here) are shown. (**B**) Representative HSF1-bound genes in M0-91 cells (*HSPA8, HSPA1B, CKS2*, and *RBM23*). x axis: from −2kb from the transcription start site (TSS) to 5 kb from the TSS for each gene. (**C**) Autoradiograph of S35 labeled protein lysates from MCF7 cells treated for 6 hrs. with the indicated concentrations of RHT or CHX. Graphs show the counts per minute from acetone precipitation of proteins in each sample, quantitated using a scintillation counter.

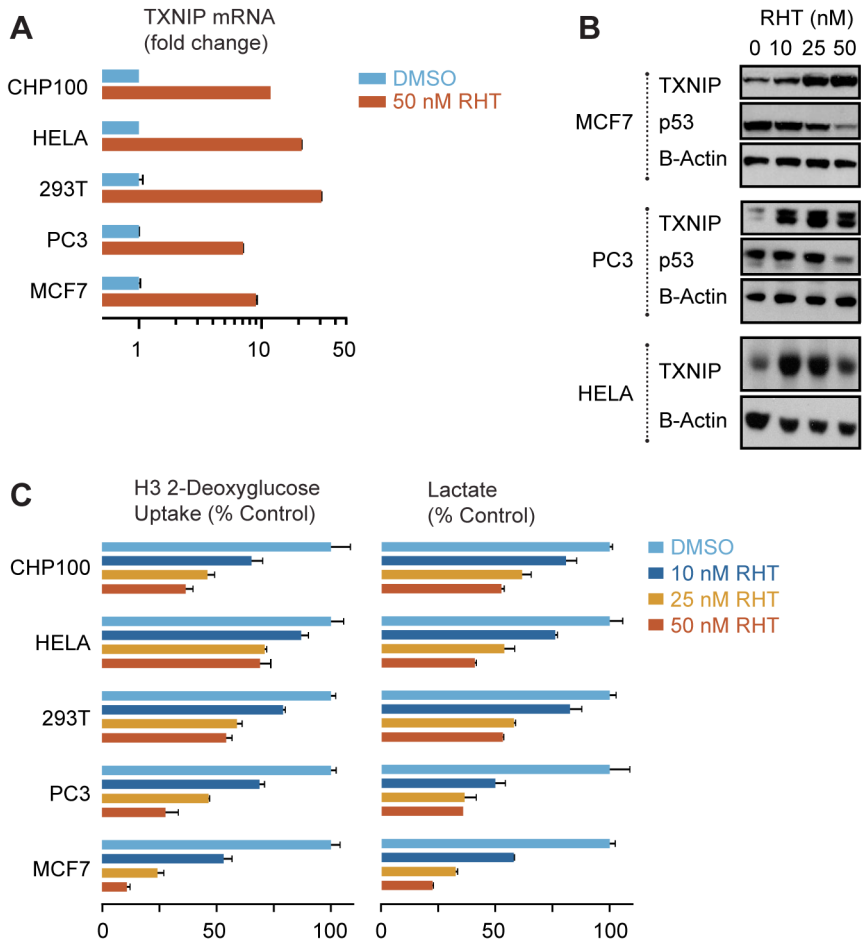

Fig. 5. Rocaglates modulate tumor energy metabolism

(**A**) TXNIP mRNA transcript levels in a panel of cancer cell lines measured by nanostring nCounter following 6 hr. incubation with 50 nM RHT. (**B**) Immunoblot showing TXNIP levels in the indicated cancer cell lines following a 6 hr. incubation with the indicated concentration of RHT. β-actin is the loading control. The effect on p53, a short half-life protein, is shown. (**C**) Effects of the indicated amount of RHT on [H3]-2-deoxyglucose uptake (left panel) and lactate production (right panel) in a panel of cancer cell lines.

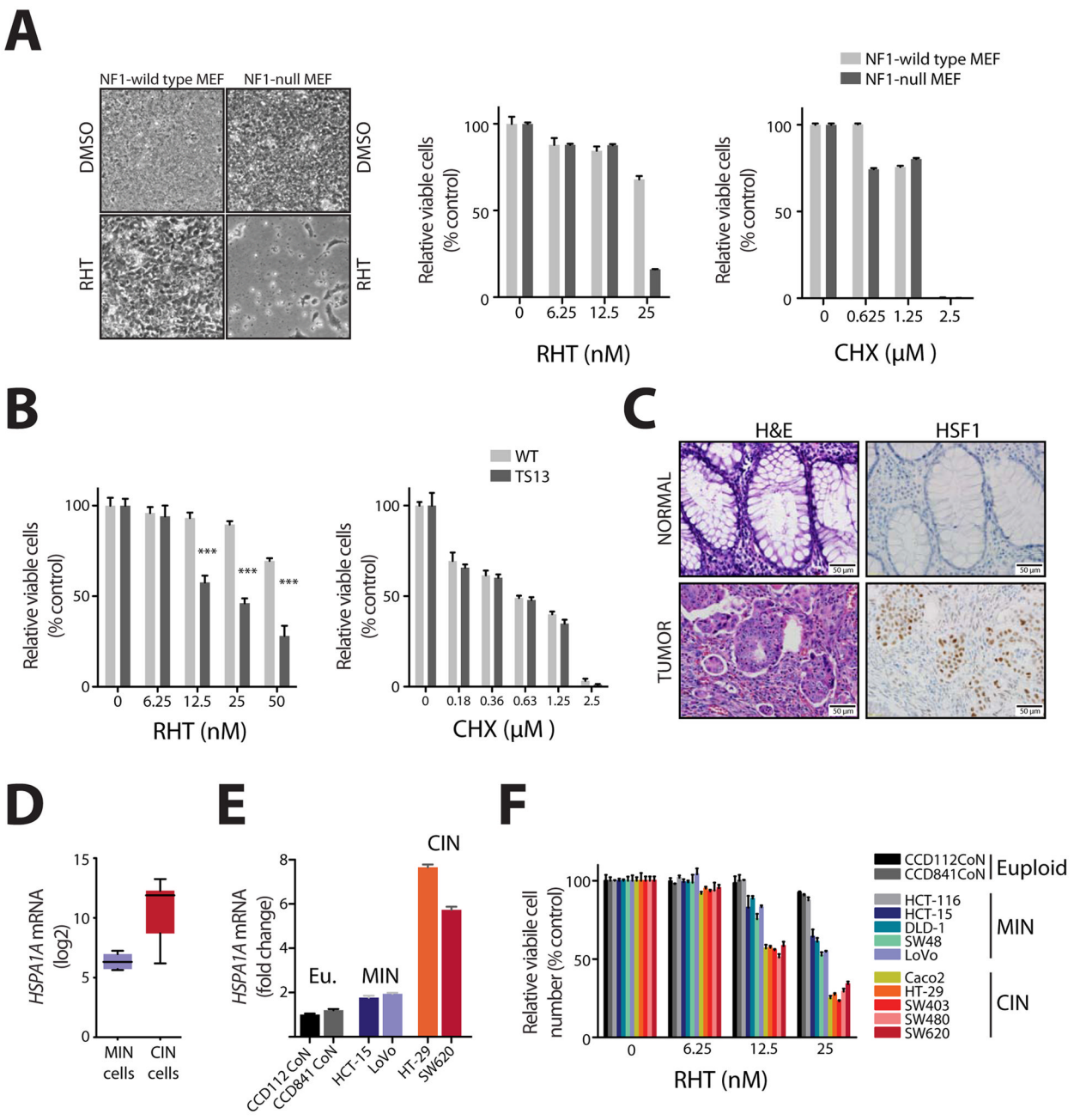

Fig. 6. Rocaglates selectively target aneuploid cancer cells and non-transformed cells with cancer-associated genetic aberrations

(A) Photomicrographs of *Nf1* wild type and *Nf1* null MEFs that were treated for 14 days with 25 nM RHT. The relative viable cell number of RHT-treated (middle panel) and CHX-treated (right panel) are shown. (**B**) Effect of either RHT (left panel) or cycloheximide (right panel) on the proliferation of MEFs (TS-13) carrying a single extra copy of 120 Mbp of chromosome 13 compared to MEFs derived from littermate controls (WT), (mean ± S.D., n=3, ***p<0.001, two-way ANOVA). (**C**) Photomicrographs of normal colon epithelial cells and invasive colon adenocarcinoma (H&E stains and HSF1 immunohistochemistry) from the same section of a human tumor resection (immunostained simultaneously). HSF1 expressing cells stain brown and HSF1 negative cells stain blue from the toluidine blue

counterstain. Scale bar: 50 μm. (**D**) *HSPA1A* mRNA transcript levels are elevated in colorectal adenocarcinomas with high-grade aneuploid karyotypes. Data from three MIN and nine CIN colon cancer cell lines from the GSK Cancer Cell Line Genomic Profiling Data as described in the methods. (**E**) RT-PCR analysis of *HSPA1A* mRNA levels in the indicated euploid, MIN and CIN cancer cell lines. (**F**) Effect of RHT on the proliferation of a panel of cell lines with high-grade aneuploid karyotypes (CIN lines: Caco2, HT29, SW403, SW480, and SW620), near-euploid karyotypes with microsatellite instability (MIN lines: HCT-116, HCT-15, DLD-1, SW48, and LoVo) or non-transformed colon epithelial cell lines with a euploid chromosomal number (CCD112CoN and CCD841CoN), (mean ± S.D., n=3, ***p<0.001, two-way ANOVA).

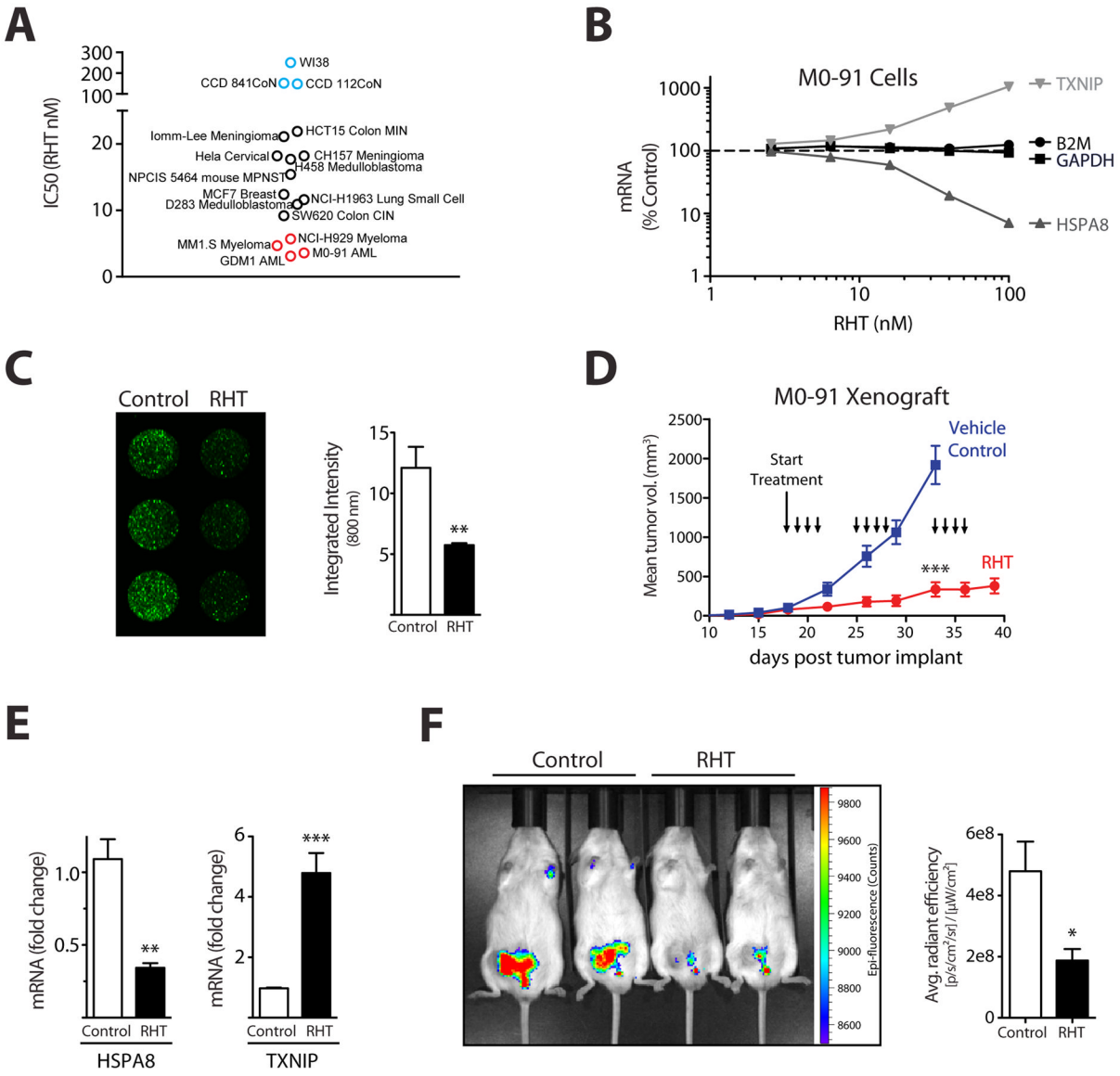

Fig. 7. Rocaglates suppress tumor growth, *HSPA8* mRNA levels and glucose uptake *in vivo*

(A) Scatter plot of IC50 values of the growth of a diverse panel of cell lines treated with RHT. Cells were treated for 5 days. Red indicates hematopoietic cancer lines and blue indicates euploid non-transformed cells. **(B)** mRNA levels of *HSPA8*, *TXNIP*, and control housekeeping genes in M0-91 cells treated with RHT. **(C)** Glucose uptake of of IR Dye 800CW 2-deoyglucose (2-DG) in M0-91 cell lines treated with RHT. Imaging was performed using LICOR. Right panel: quantitation of measured intensity (mean ± SEM, $p < .005$, two-tailed t-test). **(D)** Plot of the tumor volume of M0-91 acute myeloid leukemia xenografts treated with vehicle or RHT. The mean tumor volume (mm^3) is plotted over time. Mice were treated with subcutaneous injections starting on day 18 post-implantation (either vehicle alone or RHT (1mg/kg), on days marked by downward pointing arrows). Eight mice were in each treatment group (mean ± SE, $p < 0.0001$). **(E)** RT-PCR analysis of HSPA8 and TXNIP mRNA levels from tumor xenografts following a single treatment of either vehicle or RHT (1 mg/kg, S.C.; 5 mice in each group). Tumors were harvested 6 hrs. post-treatment (mean ± SEM, HSPA8: $p < .005$, TXNIP: $p < .0005$, two-tailed t-test). **(F)** Representative

image of epifluorescence of IRDye 800CW 2-deoxyglucose (2-DG) uptake in M0-91 xenografts. Mice bearing tumors were treated with vehicle or RHT (1 mg/kg) as described in the Materials and Methods; 4 mice in each group. Images were acquired 36 hrs. following the last treatment. Right panel: quantitation of measured radiant efficiency from epifluorescence of IRDye 800CW 2-DG from images of M0-91 xenografts (mean ± SEM, p=0.031, two-tailed t-test).